Phys Chem Minerals (2012) 39:665–674
DOI 10.1007/s00269-012-0520-1

ORIGINAL PAPER

Magnetic behavior of trioctahedral micas with different octahedral Fe ordering

Stefano Pini · Maria Franca Brigatti · Marco Affronte · Daniele Malferrari · Augusto Marcelli

Received: 7 February 2012 / Accepted: 6 June 2012 / Published online: 5 July 2012

Abstract This contribution is finalized at the discussion of the magnetic structure of two samples, belonging to phlogopite–annite [sample TK, chemical composition $^{IV}(Si_{2.76}Al_{1.24})$ $^{VI}(Al_{0.64}Mg_{0.72}$ $Fe^{2+}_{1.45}Mn_{0.03}Ti_{0.15})$ $(K_{0.96}Na_{0.05})$ $O_{10.67}$ $(OH)_{1.31}$ $Cl_{0.02}$] and polylithionite–siderophyllite joints [sample PPB, chemical composition $^{IV}(Si_{3.14}Al_{0.86})^{VI}(Al_{0.75}Mg_{0.01}$ $Fe^{2+}_{1.03}Fe^{3+}_{1.03}Mn_{0.01}Ti_{0.01}Li_{1.09})$ $(K_{0.99}Na_{0.01})$ $O_{10.00}$ $(OH)_{0.65}$ $F_{1.35}$]. Samples differ for Fe ordering in octahedral sites, $Fe^{2+}/(Fe^{2+} + Fe^{3+})$ ratio, octahedral composition, defining a different environment around Fe cations, and layer symmetry. Spin-glass behavior was detected for both samples, as evidenced by the dependency of the temperature giving the peak in the susceptibility curve from the frequency of the applied alternating current magnetic field. The crystal chemical features are associated to the different temperature at which the maximum in magnetic susceptibility is observed: 6 K in TK, where Fe is disordered in all octahedral sites, and 8 K in PPB sample, showing a smaller and more regular coordination polyhedron for Fe, which is ordered in the *trans*-site and in one of the two *cis*-sites.

Keywords Polylithionite · Siderophyllite · Crystal chemistry · XAS · Magnetic properties

Introduction

The magnetic properties of trioctahedral micas were mostly ascribed to their Fe content, which can be present as Fe^{2+} and Fe^{3+}. Depending on crystallization conditions, the $Fe^{2+}/(Fe^{2+} + Fe^{3+})$ ratio can vary significantly, together with its distribution within the layer. Fe^{3+} was found to occupy both tetrahedral and octahedral positions, whereas Fe^{2+} was located at octahedral positions only (Brigatti and Guggenheim 2002).

Coey (1985), Coey et al. (1981, 1982, 1984), and Coey and Ghose (1988) investigated the magnetic anomaly of micas at temperature close to 10 K and at high exciting magnetic fields. These contributions arise from in-plane ferromagnetic interactions between Fe^{2+} and Fe^{2+} ions connecting the magnetic structure of micas. This anomaly was also associated to the establishment of other weaker (dipole–dipole) interactions, giving antiparallel (antiferromagnetic) alignment. Ballet and Coey (1982), addressing Fe-rich 2:1 phyllosilicates, confirmed previous results and evidenced a potential magnetic ordering at T values lower than 10 K and at strong exciting magnetic field values. Furthermore, the platy morphology and the Fe arrangement were observed to enhance an anisotropic magnetic susceptibility in micas with composition close to annite. Different magnetic susceptibility values were in fact measured in-plane, where Fe atoms were found in adjacent sites, and out of plane where usually Fe-sites are bridged with non-magnetic cations (Beausoleil et al. 1983). Townsend and Longworth (1985) suggested a ferromagnetic superexchange interaction between Fe^{3+} and Fe^{3+} ions, thus

Electronic supplementary material The online version of this article (doi:10.1007/s00269-012-0520-1) contains supplementary material, which is available to authorized users.

S. Pini · M. F. Brigatti (✉) · D. Malferrari
Dipartimento di Scienze della Terra, Università di Modena e Reggio Emilia, Via S. Eufemia, 19, 41100 Modena, Italy
e-mail: mariafranca.brigatti@unimore.it

M. Affronte
Dipartimento di Fisica, Università di Modena e Reggio Emilia, Via G. Campi 213/a, 41100 Modena, Italy

A. Marcelli
INFN-LNF, Via E. Fermi 40, 00044 Frascati, RM, Italy

contrasting previous conclusions that related the observed magnetic behavior of micas to the interaction between two neighbor Fe^{3+} ions, antiferromgnetically coupled (Coey et al. 1981; Ballet and Coey 1982; Ballet et al. 1985). Some possible explanations for matching these contrasting interpretations were provided in several contributions (Coey 1985; Ballet 1986; Townsend 1987; Townsend et al. 1987; Longworth et al. 1987; Marcelli et al. 2004), without, however, reaching a final interpretation. An antiferromagnetic trend in the susceptibility − temperature curve, working in FW (field warming) mode, and a magnetic ordering at temperatures >10 K, were reported for annite crystals (Christie et al. 1992; Rancourt et al. 1994).

In trioctahedral micas, the octahedrally coordinated cations are distributed over three crystallographic positions, that is, in the *trans*-oriented M1 octahedron and in the two *cis*-oriented M2 and M3 octahedra. Octahedral cations can be completely disordered in homo-octahedral micas (M1 = M2 = M3), partially ordered in meso-octahedral (i.e., usually M1 ≠ M2, M2 = M3 in trioctahedral micas of the phlogopite–annite join or M1 = M2, M2 ≠ M3 and M1 = M3, M2 ≠ M3 in trioctahedral micas of the polylithionite–siderophyllite join) and completely ordered in hetero-octahedral micas (M1 ≠ M2 ≠ M3) (Ďurovič 1994; Nespolo and Ďurovič 2002). Lithian micas-1*M* are peculiar, since their octahedral sheet contains three vastly different cations, Li^{1+} − (Mg^{2+}, Fe^{2+}) − Al^{3+}, distributed and variously ordered in various ways in the octahedral sheet. Octahedral ordering was found to reduce symmetry from space group *C*2/*m* to *C*2 (or more precisely, referring to diperiodic groups, from *C*12/*m*(1) to *C*12(1): cf. Dornberger-Schiff et al. 1982).

The influence between Fe ordering in the octahedral sites and the magnetic behavior of trioctahedral micas was not, so far, investigated in detail. This work thus addresses the magnetic behavior of two crystals belonging to phlogopite–annite and polylithionite-siderophyllite join, respectively. These samples shows comparable total iron content, but different layer symmetry, as a consequence of different octahedral cation ordering, thus exemplifying how different cation ordering and Fe cationic environment can affect the magnetic properties in micas.

Samples and experimental methods

Samples

Sample TK, from Tinker Glacier peraluminous granites (Northern Victoria land, Antarctica), belongs to phlogopite–annite join. Sample PPB from the Precambrian Pikes Peak batholith, Southern Front Range of Colorado (west of Colorado Springs and south and southwest of Denver), belongs to polylithionite–siderophyllite join (Foord et al. 1995; Unruh et al. 1995; Kile and Foord 1998).

These samples show (1) similar total Fe content (sample TK: Fe_{total} = 1.45 apfu; sample PPB: Fe_{total} = 1.26 apfu), (2) different layer symmetry (sample TK: *C*2/*m*; sample PPB: *C*2), (3) different Fe octahedral ordering. In sample TK, Fe distribution is disordered, with a slight preference for M1 site, whereas in sample PPB, Fe together with Li occupies the *trans*-octahedral and one of the two *cis*-octahedral sites. Further crystal chemical details will be introduced when discussing single crystal X-ray diffraction and microprobe analysis results.

Chemical data

A wavelength-dispersive ARL-SEMQ microprobe (operating conditions: 15 kV accelerating voltage, 15 nA sample current, defocused electron beam of about 3 μm spot size, and counting times of 10 s for both peak and background) was used to perform electron microprobe analyses. Analyses and data reductions were executed via the probe software package of Donovan (1995). Chemical composition (Table 1) was obtained by combining the results from (1) the average of 6 microprobe point analyses, (2) H_2O determination obtained by thermal analysis (Seiko SSC 5200 thermal analyzer, heating rate 10 °C/min and Ar gas flow rate 100 μl/min), (3) information related to iron oxidation state (estimated measure standard deviation $\sigma < 4$ %, Meyrowitz 1970), (4) Li content determined by Emission Spectrometry Plasma (ICP, Varian Liberty 200). The derivation of chemical formula (Table 1), based on $O_{12-(x+y+z)}$ $(OH)_xF_yCl_z$, started from the following assumptions: (1) tetrahedral sites were considered filled with Si and Al to an occupancy of 4.0 atoms per formula unit (apfu), (2) the octahedral sites were filled with Al, Ti, Mg, Mn, Fe^{2+}, Fe^{3+}, Li, (3) Na and K were assigned to interlayer position. Furthermore, chemical formula was double-checked for consistency with data from single crystal structure refinement, namely by comparison of mean electron count in interlayer and octahedral sites independently obtained from chemical analysis and single crystal structure refinement.

Single crystal X-ray diffraction

Small crystal fragments 0.12 × 0.10 × 0.06 mm^3 (TK sample) and 0.15 × 0.12 × 0.05 mm^3 (PPB sample) were analyzed using a Bruker X8 APEX four circle diffractometer combined with APEX 4 K CCD detector, flat graphite monochromator and Mo Kα-radiation from a fine focus sealed tube. Table 2 reports refined cell-parameters and other crystal data. The SMART package was used to determine unit-cell and for X-ray data collection.

Table 1 Averaged chemical composition, chemical formulae based on (O_{12-x-y} $(OH)_xF_y$) and mean atomic number (man) for Mg-rich annite (sample TK) and Li-rich siderophyllite (sample PPB)

Sample	TK	PPB		TK	PPB
Chemical composition (oxide wt%)			*Chemical formula* (apfu)		
SiO_2	34.52	41.19	Tetrahedral cations		
TiO_2	2.50	0.12	Si	2.76	3.14
Al_2O_3	20.00	17.99	Al	1.24	0.86
Fe_2O_3	bdt	2.20	Octahedral cations		
FeO	21.75	16.15	Al	0.64	0.75
ZnO	bdt	0.02	Mg	0.72	0.01
MnO	0.44	0.20	Fe^{3+}		0.13
MgO	6.03	0.10	Fe^{2+}	1.45	1.03
Li_2O	bdt	3.58	Mn^{2+}	0.03	0.01
Na_2O	0.29	0.10	Ti^{4+}	0.15	0.01
K_2O	9.41	10.20	Li^{+}		1.09
F	bdt	5.60	Interlayer cations		
Cl	0.12	bdt	Na	0.05	0.01
H_2O	4.95	2.50	K	0.96	0.99
Sum	100.01	99.95	Anions		
			F		1.35
Mean atomic number (*man*)			Cl	0.02	
Octahedral sites			OH	1.31	0.65
$M1_{(Xref)}$	20.0(8)	14.6(1)	O	10.67	10.00
$M2_{(Xref)}$	19.1(1)	14.1(1)			
$M3_{(Xref)}$	19.1(1)	14.7(2)			
$M1 + M2 + M3_{(Xref)}$	58.2	43.4			
$M1 + M2 + M3_{(Epma)}$	58.7	43.8			
Interlayer site					
$A_{(Xref)}$	18.9(7)	19			
$A_{(Epma)}$	18.7	18.9			

bdt Below detection threshold

Redundant data were collected for an approximate sphere of reciprocal space and were integrated and corrected for background and Lorentz-polarization factors using the Bruker program SAINT+ (Bruker 1999a). The Bruker SADABS (Bruker 1999b) package was used to make the semi-empirical absorption correction. The crystal structure was refined using the SHELX-97 software package (Sheldrick 1997) in the space group *C*2/*m* (TK sample) and *C*2 (PPB sample) with neutral atomic scattering factors starting from the atomic coordinates of Brigatti et al. (2000) and Brigatti et al. (2005). Table 3 lists selected interatomic distances and parameters obtained from the structure refinement. The mean electron counts for octahedral and interlayer sites, determined following crystal structure refinement and electron microprobe analysis, are listed in Table 1. Atomic coordinates, isotropic and anisotropic displacement parameters as well as observed and calculated structure factors are available from the authors upon request.

X-ray absorption spectroscopy (XAS)

Fe *K*-edge XAS spectra were collected at ESRF European Synchrotron Radiation Facilities (ESRF, Grenoble, France) on the beamline BM-25 (SpLine, Spanish Beam Line). The storage ring conditions were 6 GeV working in the current range 180–200 mA. A Si(111) double-crystal monochromator was used, providing an energy resolution of ~0.4 eV at the Fe *K*-edge, which is much less than the Fe *K* natural line width (~1.15 eV; Krause and Oliver 1979). For all spectra, a metallic Fe reference foil was used to provide an energy calibration for the monochromator (energy reproducibility: ±0.05 eV). Data were collected in fluorescence mode at room conditions. Spectra were recorded over a range of 500 eV across the Fe absorption *K*-edge with 1 eV energy step in the edge region (7,100–7,150 eV) and 3 eV in the extended X-ray absorption fine structure (EXAFS) region (7,150–7,500 eV). Phlogopite, containing only a small

Table 2 Crystallographic data and refinement results for Mg-rich annite (sample TK) and Li-rich siderophyllite (sample PPB)

	TK	PPB		TK	PPB
a (Å)	5.3482(9)	5.3060(5)	Measured reflections	2,372	2,096
b (Å)	9.274(2)	9.1636(9)	Unique reflections	621	1,070
c (Å)	10.229(2)	10.116(1)	Refined parameters	57	97
β (°)	100.174(9)	100.786(4)	Completeness (%)	96.1	86.5
V (Å^3)	499.4(2)	483.17(8)	R [$I > 2\sigma(I)$]	3.65	3.94
Space group	$C2/m$	$C2$	wR^2 [I > 2σ(I)]	8.52	7.78
Crystal size (mm)	0.12 × 0.10 × 0.06	0.34 × 0.13 × 0.03	R_{int}	2.76	2.82
h, k, l ranges	h: −6 → 6,	h: −6 → 7,	GOF	0.988	0.986
	k: −11 → 11,	k: −13 → 10,			
	l: −13 → 13	l: −14 → 12			
θ range (°)	4–28	4–31			

$R = \frac{\sum ||F_o|-|F_c||}{\sum |F_o|} \times 100$, $wR^2 = \left[\frac{\sum w\left(F_o^2-F_c^2\right)^2}{\sum w\left(F_o^2\right)^2}\right]^{1/2} \times 100$, GOF $= \left[\frac{\sum w\left(F_o^2-F_c^2\right)^2}{(n-p)}\right]^{1/2}$

$w = 1/[\sigma^2(F_o^2) + (a \times P)^2 + b \times P]$, where $a = 0.0616$ for sample TK and 0.0440 for sample PPB, respectively, $b = 0$, $P = [(\max(F_o^2, 0) + 2 \times F_c^2)]/3$; n is the number of reflections, and p is the number of parameters refined

amount of Fe^{2+} in M1 site, tetra-ferriphlogopite, containing mostly Fe^{3+} in tetrahedral sites and annite characterized by a full occupancy of Fe^{2+} in the octahedral sites were collected as additional standards and to interpret the spectra.

Magnetic measurements

A Quantum Design PPMS-7T cryomagnetic system installed at S3 laboratories (CNR-Institute of Nanosciences located at the Departments of Physics of University of Modena and Reggio Emilia) was used to perform studies of heat capacity and magnetic susceptibility in the temperature range 2.2–300 K and in magnetic fields of 10 Oe on 36 mg of powdered mica sample. The measurements were carried out in field cooling. Molar magnetic susceptibility χ' ($\chi = C/T$) was expressed in emu mol^{-1}. In particular, C is the Curie constant $\left(C = \frac{Ng^2\mu_B^2 S(S+1)}{3k_B}\right)$, where N = number of iron ions/g of mineral ($N = 3.03 \times 10^{-3}$ and 2.52×10^{-3} mol g^{-1}, for TK and PPB samples, respectively); μ_B = Bohr magneton (9.274015×10^{-21} erg G^{-1}); g = gyromagnetic ratio ($g = 2.0023$); S = spin angular momentum ($S = 5/2$ for Fe $^{3+}$ and $S = 2$ for Fe^{2+}); k_B = Boltzman constant ($k_B = 1.38 \times 10^{-16}$ erg K^{-1}).

Results and discussion

Crystal chemistry and XANES spectroscopy

Chemical formulae (Table 1) for samples TK and PPB are $^{IV}(Si_{2.76}Al_{1.24})$ $^{VI}(Al_{0.64}Mg_{0.72}Fe^{2+}_{1.45}Mn_{0.03}Ti_{0.15})$ $(K_{0.96}Na_{0.05})$ $O_{10.67}$ $(OH)_{1.31}$ $Cl_{0.02}$ and $^{IV}(Si_{3.14}Al_{0.86})$-$^{VI}(Al_{0.75}Mg_{0.01}Fe^{2+}_{1.03}Fe^{3+}_{1.03}Mn_{0.01}Ti_{0.01}Li_{1.09})$ $(K_{0.99}Na_{0.01})$ $O_{10.00}$ $(OH)_{0.65}F_{1.35}$, respectively. According to the nomenclature of the micas (Rieder et al. 1998), sample TK is a Mg-rich annite, whereas sample PPB is a Li-rich siderophyllite. Total Fe content is similar in both samples, despite the different Fe^{2+}/Fe^{3+} ratio and a significantly different octahedral composition, since PPB sample is richer in Li and poorer in Mg with respect to TK sample, thus giving a remarkably different surrounding for Fe.

The crystal structure refinement suggests the space group $C2/m$ for sample TK, whereas, following from Al ordering in one of the two *cis*-sites (M2), the layer symmetry reduces to the space group $C2$ for sample PPB. Sample TK presents the octahedral mean bond distances values ⟨M1–O⟩ = 2.098 Å, ⟨M2–O⟩ = ⟨M3–O⟩ = 2.069 Å), and the mean electron counts (mec) values mec M1 = 20.0(8) and mec M2 = mec M3 = 19.1(1). Sample PPB shows two octahedral sites (M1 and M3) close both in size (⟨M1–O⟩ = 2.135 Å, ⟨M3–O⟩ = 2.129 Å) and in mean electron count [mec M1 = 14.6(1) and mec M3 = 14.7(2)]. The remaining *cis*-octahedral site is characterized by a shorter ⟨M–O⟩ distance (⟨M2–O⟩ = 1.915 Å) and a by a mec value of 14.1(1). The size and the mec of the octahedral sites also suggest that Fe^{2+} is mainly located in two of the three octahedral sites (M1 and M3) for PPB sample and disordered in TK, albeit with a preference for the M1 site.

Further information on Fe local distribution inside the structure was obtained by X-ray absorption near edge structure spectroscopy (XANES). Spectra were collected at the iron *K*-edge both on samples under study and on three natural well-studied micas (phlogopite, tetra-ferriphlogopite

Table 3 Bond distances (Å) and parameters derived from structure refinement for Mg-rich annite (sample TK, space group *C*2/*m*) and Li-rich siderophyllite (sample PPB, space group *C*2)

Sample TK		Sample PPB			
Tetrahedron (T1)		*Tetrahedron* (T1)			
T1–O1	1.659(1)	T1–O1	1.660(9)	Sample TK	
T1–O2	1.662(2)	T1–O2	1.634(7)	*Tetrahedral parameters*	
T1–O2′	1.659(2)	T1–O22	1.621(7)	α (°)	7.39
T1–O3	1.673(2)	T1–O3	1.645(7)	Δ*z* (Å)	0.023
⟨T1–O⟩	1.663	⟨T1–O⟩	1.640	τ(T1) (°)	110.2
Octahedron (M1)		*Tetrahedron* (T2)		Tetrahedral thickness (Å)	2.231
M1–O3 (×4)	2.109(2)	T11–O1	1.626(9)	*Octahedral parameters*	
M1–O4 (×2)	2.077(3)	T11–O2	1.664(7)	⟨O3–O3⟩ (Å)	3.090
⟨M1–O⟩	2.098	T11–O22	1.657(6)	σ⟨O3–O3⟩ (Å)	0.025
Octahedron (M2 = M3)		T11–O33	1.646(6)	M1–O4–M2 (°)	97.02(6)
M2–O3 (×2)	2.077(2)	⟨T11–O⟩	1.648	M1–O4–M2′ (°)	97.02(6)
M2–O3′ (×2)	2.084(2)	*Octahedron* (M1)		M2–O4–M2 (°)	109.55(5)
M2–O4 (×2)	2.045(2)	M1–O3 (×2)	2.111(8)	M1–O3–M2′ (°)	121.15(8)
⟨M2–O⟩	2.069	M1–O33 (×2)	2.158(7)	*Octahedral thickness*	2.105
Interlayer cation		M1–O4 (×2)	2.135(3)		
A–O1 (×2)	3.000(3)	⟨M1–O⟩	2.135	Sample PPB	
A–O2 (×4)	3.001(2)	Octahedron (M2)		Tetrahedral parameters	
A–O2′ (×4)	3.334(2)	M2–O3 (×2)	1.958(8)	α (°)	3.80
A–O1′ (×2)	3.357(3)	M2–O33 (×2)	1.925(5)	Δ*z* (Å)	0.091
$\langle A–O\rangle_{inner}$	3.001	M2–O4 (×2)	1.861(5)	τ(T1) (°)	111.04
$\langle A–O\rangle_{outer}$	3.342	⟨M2–O⟩	2.135	τ(T2) (°)	111.11
A–O4	4.011(2)	Octahedron (M3)		*Tetrahedral thickness* (Å)	2.251
		M3–O3 (×2)	2.122(6)	*Octahedral parameters*	
		M3–O33 (×2)	2.099(8)	⟨O3–O3⟩	3.064
		M3–O4 (×2)	2.167(5)	σ⟨O3–O3⟩ (Å)	0.184
		⟨M3–O⟩	2.129	M1–O4–M2 (°)	100.17(6)
		A–O1 (×2)	3.056(3)	M1–O4–M3 (°)	91.20(6)
		A–O1′ (×2)	3.248(3)	M2–O4–M3 (°)	100.21(6)
		A–O2 (×2)	3.035(7)	M1–O3–M2 (°)	93.14(6)
		A–O2′ (×2)	3.252(8)	M1–O3–M3′ (°)	97.36(7)
		A–O22 (×2)	3.047(7)	*Octahedral thickness*	2.100
		A–O22′ (×2)	3.148(7)		
		$\langle A–O\rangle_{inner}$	3.046		
		$\langle A–O\rangle_{outer}$	3.216		
		A–O4	3.966(2)		

Estimated standard deviations in parenthesis

and annite, Tombolini et al. 2002; Giuli et al. 2001) to obtain information on the Fe oxidation state, on Fe coordination number and on local geometry around the absorber. Standards analyzed (Fig. 1) were chosen because of their similarity in topology to samples under study and because of the different iron oxidation and distribution into the layer (i.e., phlogopite presents a low Fe^{2+} content in octahedral M1 site, tetra-ferriphlogopite presents Fe^{3+} mostly in tetrahedral coordination and annite presents Fe^{2+} in all octahedral sites). In both TK and PPB samples, the pre-edge feature at 7,115.5 eV (feature A, Fig. 1), which is well evident in tetra-ferriphlogopite and ascribed to Fe^{3+} for Si substitution, is negligible, thus suggesting that Fe^{3+} content observed in sample PPB ($Fe^{3+} = 0.13$ apfu) could be assigned to octahedral coordination only (Waychunas et al. 1983; Wilke et al. 2001). The energy position of the threshold structure, well evident in tetra-ferriphlogopite (7,124.5 eV, feature B), is consistent with

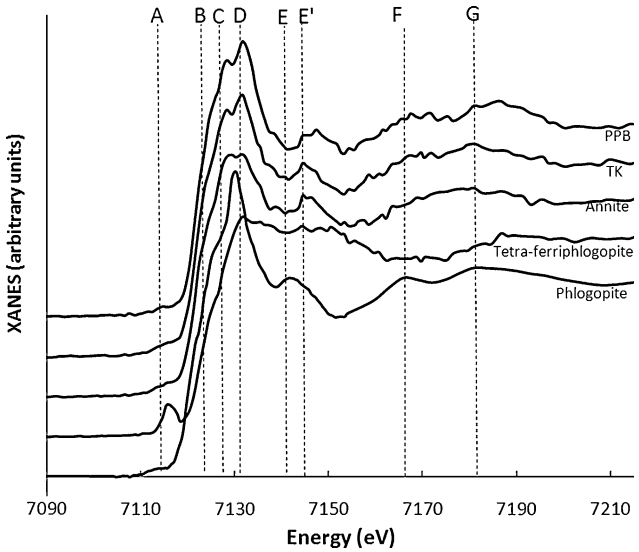

Fig. 1 Fe *K*-edge XANES spectra of Mg-rich annite (sample TK) and Li-rich siderophyllite (samples PPB) compared with phlogopite, tetra-ferriphlogopite and annite

limited (sample PPB) or negligible (sample TK) Fe^{3+} content.

Information on Fe^{2+} distribution in the octahedral sites can be derived from the comparison of C, D, E (E′), F and G features in TK and PPB spectra with respect to both phlogopite and annite. The intensity ratio between C and D effects at 7,128.3 and 7,131.6 eV, respectively, suggests similar Fe content in TK and PPB samples. Feature E can be related to Fe^{2+} ordering in octahedral sites (Tombolini et al. 2002). This feature occurs at 7,140.3 and at 7,144.5 eV in phlogopite (feature E) and annite (feature E′), respectively. In phlogopite, Fe^{2+} is limited and ordered at M1 site only, unlike in annite, where Fe^{2+} entirely occupies all the octahedral positions. Sample TK shows feature E′ very close to annite, thus suggesting Fe disordered distribution in all octahedral sites. The similarity can be also observed for sample PPB, where the shift of E′ peak at 7,147.4 eV and its broadening could be associated to Fe ordered in M1 and M3 sites only, as hinted by crystal structure refinement. Although the critical signal to noise ratio, the spectral range between 7,160 and 7,200 eV shows an upward bending in annite, phlogopite, TK and PPB samples. This band, clearly doubled in phlogopite (features F and G at 7,166.0 and 7,181.0 eV), where Fe is mostly located at M1, is also doubled, even more evidently, in sample PPB, possibly as a consequence of Fe preferential ordering in M1 and M3 octahedral sites (Fig. 3 in Tombolini et al. 2002).

Structural refinement, chemical analysis and XAS evidences thus suggest the following cation distribution in octahedral sites: (1) sample TK: M1 = $Fe^{2+}_{0.600}$ $Mg_{0.400}$; M2 = M3 = $Al_{0.320}Mg_{0.160}$ $Fe^{2+}_{0.425}$ $Ti_{0.075}Mn_{0.015}$, (2) sample PPB: M1 = $Fe^{2+}_{0.515}$ $Li_{0.460}$ $\square_{0.025}$; M2 = $Al_{0.750}$ $Mg_{0.010}$ $Fe^{3+}_{0.130}Li_{0.130}$ $Mn_{0.010}Ti_{0.010}$; M3 = $Fe^{2+}_{0.515}$ $Li_{0.500}$. To resume, in both samples M1 site is occupied by Fe together with mostly Mg in TK sample and Li in PPB sample. In the TK sample, both the *cis*-sites are occupied also by Fe, unlike in sample PPB, where Fe^{2+} is located in only one of the two *cis*-sites (M3). Al distribution is complementary to Fe and thus located in both *cis*-octahedral sites in TK sample and in only one of the two *cis*-sites (M2) in PPB sample.

Magnetic behavior

Fe is the main magnetic element significantly present in both samples (sample TK: $Fe^{2+} = 1.45$ apfu, Fe = 3.03×10^{-3} mol/g; sample PPB: $Fe^{2+} = 1.03$ apfu, $Fe^{3+} = 0.13$, Fe = 2.52×10^{-3} mol/g—Table 1). In trioctahedral micas with relevant octahedral Fe content, such as annite, the principal magnetic interaction is super-exchange. This interaction is strong only for nearest-neighbor cations sharing a common oxygen ligand, such as in Fe^{2+}-rich trioctahedral micas, where Fe atoms are located at adjacent M1 and M2 sites, or possibly else at two adjacent M2 sites. The sign of the super-exchange interaction can be usually inferred from cation–anion–cation bond angles. In particular, Fe^{2+}–O–Fe^{2+} interactions are expected to be negative for bond angles close to 180° and weakly positive for bond angles close to 90° (Coey and Ghose 1988). The angles defined by two octahedral cations and a shared oxygen atom ranges from 97.02(6)° (M1–O4–M2) to 121.15(8)° (M1–O3–M2′) and from 91.20(6)° (M1–O4–M3) to 100.21(6)° (M2–O4–M3) in sample TK and PPB, respectively (Table 3). Thus, super-exchange interactions in both samples are likely ferro-magnetic. Coey et al. (1981) proposed that the magnetic structure of phyllosilicates with a magnetic behavior similar to that found for the sample TK can be explained by the confinement of Fe atoms in a bi-dimensional structure, that is, in the octahedral sheet. Along the sheet, the magnetic moments of individual atoms (lying in the plane defined by the crystallographic directions **a***, **b***) are coupled by super-exchange ferromagnetic interactions, but individual octahedral sheets would be coupled by antiferromagnetic dipole–dipole interactions, instead.

Sample TK shows that, at high temperatures, the magnetic susceptibility follows the typical paramagnetic behavior. The maximum in the susceptibility observed at low temperatures ($T = 6$ K) in Fig. 2a, suggests, according to previous studies (Rancourt et al. 1994), an incipient ordering at lower-temperatures. The Weiss θ constant, determined by extrapolation of the best fit intercept of the

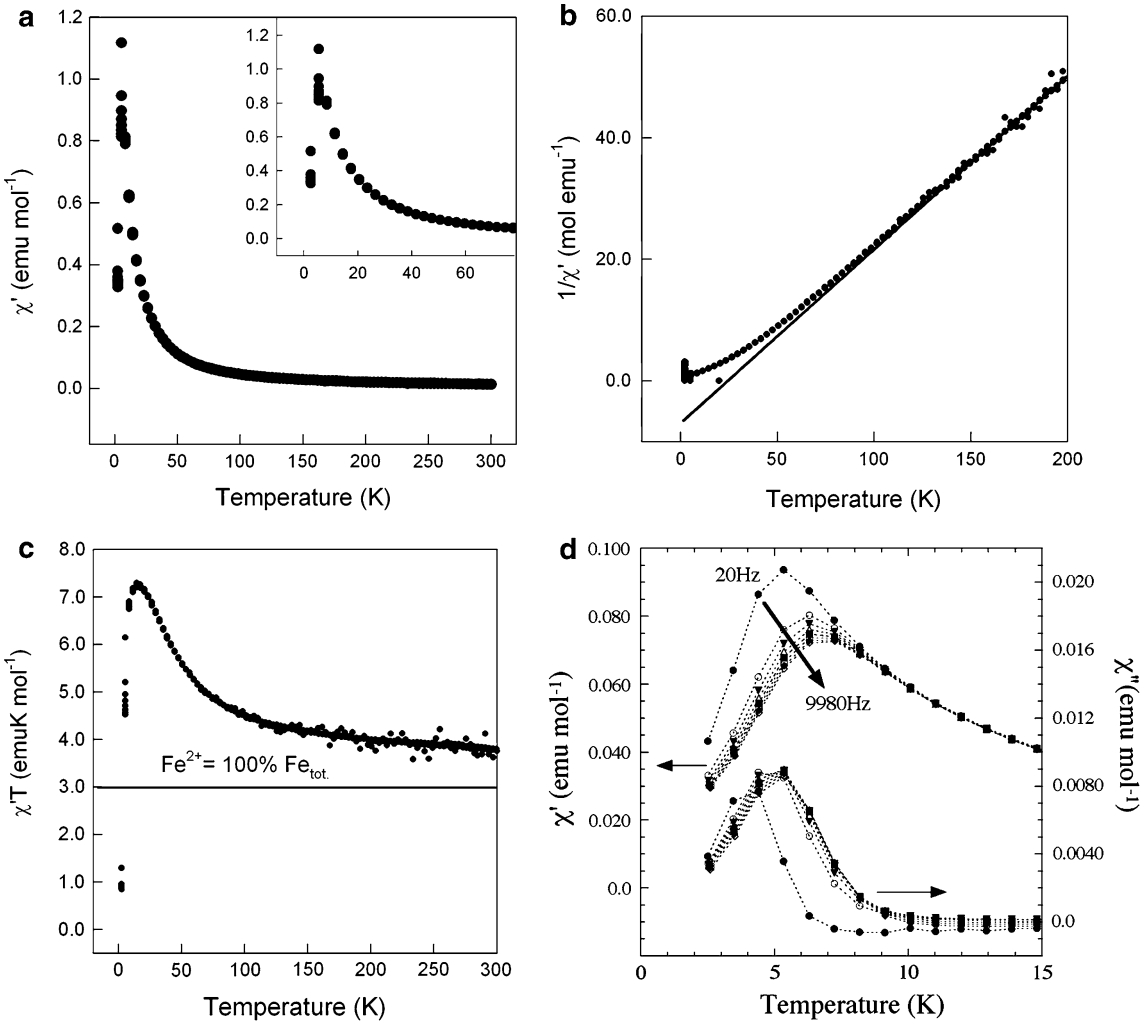

Fig. 2 Mg-rich annite (sample TK). **a** Trend of the real component of the magnetic susceptibility (χ') versus temperature, measured at $H = 10$ Oe in Field Cooling. **b** Inverse of the real component of the magnetic susceptibility ($1/\chi'$) versus temperature; the *solid line* represents the linear fit of the curve in the region of temperature between 80 and 200 K. **c** $\chi' \times T$ versus temperature; the *solid line* represents the theoretical product. **d** Trend between 0 and 15 K of real (χ') and imaginary (χ'') components (first harmonic) of the magnetic susceptibility as a function of temperature and frequency (*filled circles* 20 Hz, *open circles* 1,442.9 Hz, *filled triangle down* 2,865.8 Hz, *open triangle up* 4,288.7 Hz, *filled square* 5,711.6 Hz, *open square* 7,134.5 Hz, *filled diamond* 8,557 Hz, *open diamond* 9,980.3 Hz)

$1/\chi'$ versus T curve (Fig. 2b), is approximately 19 K, thus indicating that the exchange interactions are predominantly ferromagnetic. The positive value of the Weiss constant θ is also confirmed by the plot ($\chi' \times$ T, vs. T) (Fig. 2c), which shows an upturn of $\chi' \times$ T with temperature lowering. These results therefore suggest, for sample TK, a predominant ferromagnetic exchange interaction.

Spin glass is a disordered magnetic system, showing bulk magnetic ordering at low temperature (Binder and Young 1986). Spin-glass condition can be defined as a magnetic system with a random, yet cooperative, spin freezing, which occurs at a well-defined temperature (freezing temperature). This system originates when magnetic atoms are randomly incorporated into a not magnetic host. When freezing temperature is reached, the system evolves toward a condition that, even though not ordered, exhibits slow magnetic behavior and memory effects. Thus, spin-glass systems can be detected, for instance, by frequency dependent peak in the susceptibility curve when an AC magnetic field is applied (Binder and Young 1986). Figure 2d shows the temperature variation of both the real and the imaginary component of susceptibility in the range 0–15 K, at 8 different frequencies, corroborating the presence of a spin-glass pattern.

Figure 3a reports the variation of magnetic susceptibility in sample PPB as a function of temperature. This curve

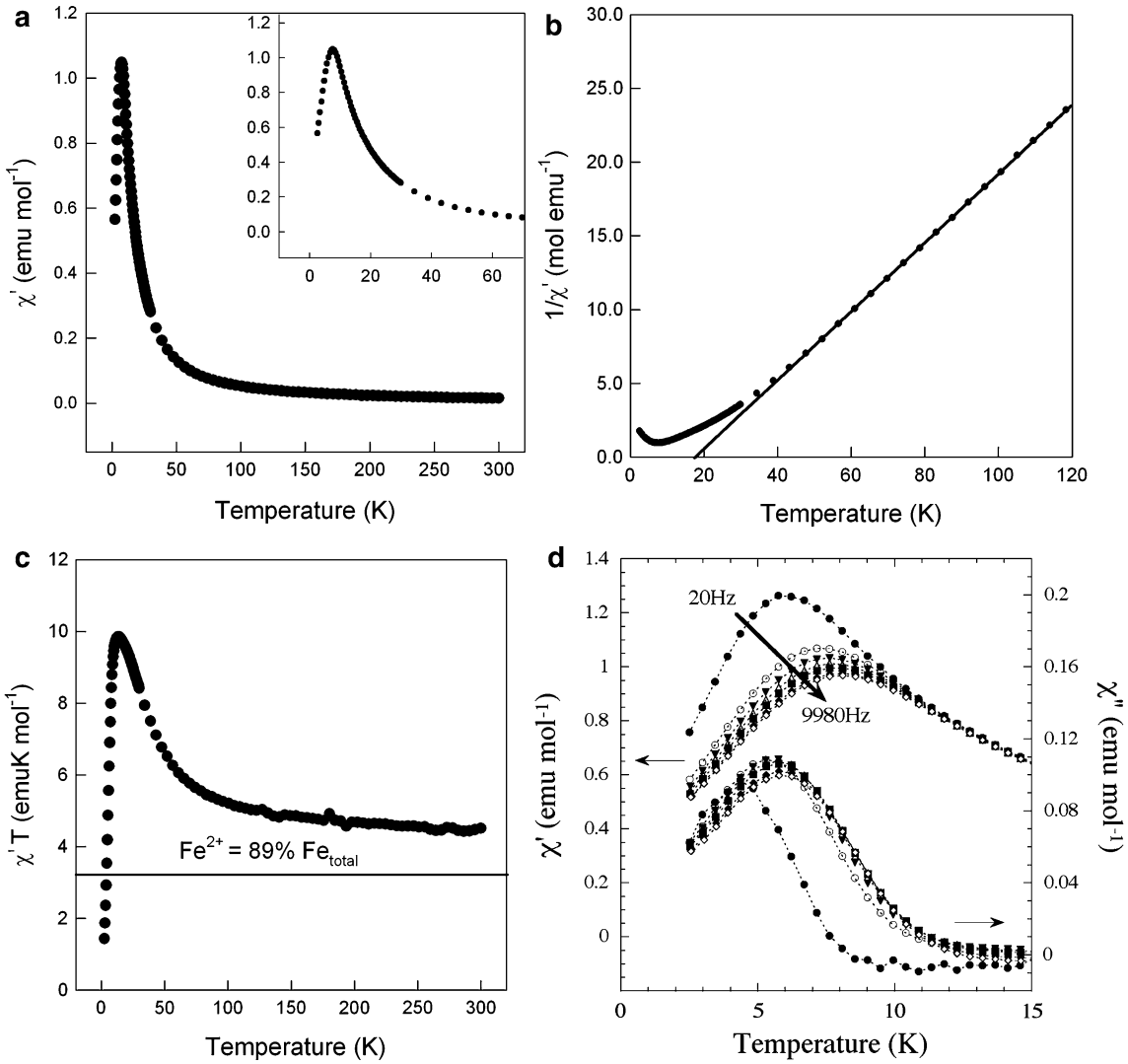

Fig. 3 Li-rich siderophyllite (sample PPB). **a** Trend of the real component of the magnetic susceptibility (χ') versus temperature, measured at $H = 10$ Oe in field cooling. **b** Inverse of the real component of the magnetic susceptibility ($1/\chi'$) versus temperature; the *solid line* represents the linear fit of the *curve* in the region of temperature between 80 and 200 K. **c** $\chi' \times T$ versus temperature; the *solid line* represents the theoretical product. **d** Trend between 0 and 15 K of real (χ') and imaginary (χ'') component of the magnetic susceptibility as a function of temperature and frequency (*filled circles* 20 Hz, *open circles* 1,442.9 Hz, *filled triangle down* 2,865.8 Hz, *open triangle up* 4,288.7 Hz, *filled squares* 5,711.6 Hz, *open squares* 7,134.5 Hz, *filled diamond* = 8,557 Hz, *open diamond* 9,980.3 Hz)

evidences a peak in susceptibility, like in TK sample, but at higher temperature (8 K). This feature could be explained by the more ordered Fe distribution, which, as previously discussed, is mostly located in the two symmetry independent M1 and M3 octahedral sites in PPB sample. A similar magnetic behavior, when discussing magnetic features of sample TK, was interpreted starting from the model introduced by Coey et al. (1981). However, the limited amount of material available, for both TK and PPB samples, prevented a neutron diffraction analysis, which could confirm (or deny) for each sample a long-range ordering.

Figure 3b, c demonstrate that, also in PBB sample, the predominant interactions inside layers are ferromagnetic. The inverse of the susceptibility curve well approximates Curie law at high temperature and defines a positive Weiss constant ($\theta = 17$). Furthermore, the $\chi' \times T$ product is always above the theoretical value calculated at $\theta = 0$ for the PBB sample.

The peak in both χ' and χ'' noticeably shifts toward higher temperature values as frequency is increased (Figs. 2d, 3d), thus suggesting a spin-glass behavior for both samples (Binder and Young 1986). Two factors may account for the absence of long-range ordering: (1) the distance between two adjacent layers containing Fe may be long enough to reduce the interaction from sheet to sheet and consequently destroying ordering. However, this

hypothesis could not be confirmed from the literature data (Ballet et al. 1985; Coey 1987), (2) Fe^{3+} may be present thus destroying the anti-ferromagnetic ordering and weakening the ferromagnetic one inside octahedral sheets, because of the negative Fe^{3+}–O–Fe^{3+} super-exchange interaction. At low concentration, isolated Fe^{3+} ions may thus not be effective in breaking the ferromagnetic ordering. However, when Fe^{3+} is significantly present in mineral structure, the Fe^{3+}–Fe^{3+} pairs may induce a weakening of the ferromagnetic alignment inside octahedral sheets (Ballet et al. 1985).

Concluding remarks

Both micas considered, belonging to the series phlogopite–annite and polylithionite–siderophyllite present a similar total Fe content, all located in octahedral coordination. Samples differ for Fe ordering in octahedral sites, $Fe^{2+}/(Fe^{2+}+Fe^{3+})$ ratio, octahedral composition, defining a different environment around Fe cations, and layer symmetry. Both samples show at low temperature and at weak applied magnetic fields a maximum in magnetic susceptibility: at $T = 5.5$ K for sample TK and at significantly higher temperature for sample PPB ($T = 8$ K). This experimental result well matches a more regular and smaller coordination polyhedron for Fe^{2+} observed in PPB sample with respect to TK.

Super-exchange interactions are present in both samples; furthermore, the strength of these interactions, evaluated by the Curie–Weiss constant, is higher in sample TK ($\theta = 19$) compared to sample PPB ($\theta = 17$). This evidence, according to the literature results (Rancourt et al. 1994), could be attributed to $Fe^{2+}/(Fe^{2+} + Fe^{3+})$ in the octahedral position. Both samples were observed to miss a long-range magnetic ordering, establishing a spin-glass behavior, as a consequence of the presence of not magnetic element surrounding Fe in both samples and to Fe^{3+} in sample PPB, breaking long-range ordering according to the evidences of Ballet et al. (1985). It is worth noting that the number of Fe cations in octahedral coordination is lower than observed in the literature samples showing a planar anti-ferromagnetic behavior.

Acknowledgments We would kindly acknowledge Italy's Ministero dell'Istruzione Università e Ricerca (Project PRIN 2008) and Fondazione Cassa di Risparmio di Modena (International Project 2010) for their financial support. The European Synchrotron Radiation Facility (ESRF) is also acknowledged for the beam-time availability and Dr. German Castro and SpLine (BM25, Spanish Beamline) staff for their valuable help during the acquisition of XAS spectra. An appreciated support was also provided by Centro Interdipartimentale Grandi Strumenti (CIGS) of Modena and Reggio Emilia University and by its staff. Thanks is also due to D. Kile and A. Rossi for sample supplying.

References

Ballet O (1986) Comment on magnetism in biotites. Phys Chem Miner 13:281. doi:10.1007/BF00308281

Ballet O, Coey JMD (1982) Magnetic properties of sheet silicates; 2:1 layer minerals. Phys Chem Miner 8:218–229. doi:10.1007/BF00309481

Ballet O, Coey JDM, Mangin P, Townsend MG (1985) Ferrous talc—a planar antiferromagnet. Solid State Commun 55(9):787–790. doi:10.1016/0038-1098(85)90798-7

Beausoleil N, Lavallèe P, Yelon A, Ballet O, Coey JMD (1983) Magnetic properties of biotite micas. J Appl Phys 54:906–915. doi:10.1063/1.332053

Binder K, Young AP (1986) Spin glasses: experimental facts, theoretical concepts and open questions. Rev Mod Phys 58:801–976. doi:10.1103/RevModPhys.58.801

Brigatti MF, Guggenheim S (2002) Mica crystal chemistry and the influence of pressure, temperature, and solid solution on atomistic models. In: Mottana A, Sassi FP, Thompson JB Jr, Guggenheim S (eds) Micas: crystal chemistry and metamorphic petrology, vol 46. Mineralogical Society of America, Washington, DC, pp 1–98. doi:10.2138/rmg.2002.46.01

Brigatti MF, Lugli C, Poppi L, Foord EE, Kile DE (2000) Crystal chemistry variation in Li- and Fe-rich micas from pikes peak batholith (central Colorado). Am Miner 85:1275–1286. ISSN: 0003-004X

Brigatti MF, Caprilli E, Funiciello R, Giordano G, Mottana A, Poppi L (2005) Crystal chemistry of ferroan phlogopites from the Albano maar lake (Colli Albani volcano, central Italy). Eur J Miner 17(4):611–621. doi:10.1127/0935-1221/2005/0017-0611

Bruker AXS (1999a) SAINT+ (version 6.01). Bruker AXS, Madison

Bruker AXS (1999b) SADABS (version 2.03). Bruker/Siemens area detector absorption and other corrections. Bruker AXS, Madison

Christie IAD, Rancourt DG, Lamarche G, Royer M, Kodama H, Robert J-L (1992) Low temperature Mössbauer spectroscopy and magnetism of synthetic annite mica. Hyperfine Interact 68(1–4):315–318. doi:10.1007/BF02396499

Coey JMD (1985) Magnetic order in trioctahedral sheet silicates: a review. In: Proceedings of the international clay conference, Denver, pp 261–266

Coey JMD (1987) New permanent magnet materials. Phys Scr T19B:426–434. doi:10.1088/0031-8949/1987/T19B/017

Coey JMD, Ghose S (1988) Magnetic ordering and thermodynamics in silicates. NATO ASI Ser Ser C Math Phys Sci 225:459–499

Coey JMD, Ballet O, Moukarika A, Soubeyroux JL (1981) Magnetic properties of sheet silicates; 1:1 layer minerals. Phys Chem Miner 7:141–148. doi:10.1007/BF00308232

Coey JMD, Moukarika A, Ballet O (1982) Magnetic order in silicate minerals. J Appl Phys 53((11, Pt 2)):8320–8325. doi:10.1063/1.330353

Coey JMD, Chukhrov FV, Zvyagin BB (1984) Cation distribution, Mössbauer spectra, and magnetic properties of ferripyrophyllite. Clays Clay Miner 32(3):198–204. doi:10.1346/CCMN.1984.0320307

Donovan JJ (1995) PROBE: PC-based data acquisition and processing for electron microprobes. Advanced Microbeam, 4217 King Graves Rd, Vienna, Ohio, 44473

Dornberger-Schiff K, Backhaus K-O, Ďurovíč S (1982) Polytypism of micas: OD-interpretation, stacking symbols, symmetry relations. Clays Clay Miner 30:364–374. doi:10.1346/CCMN.1982.0300507

Ďurovič S (1994) Classification of phyllosilicates according to the symmetry of their octahedral sheet. Ceram-Silikáty 38:81–84

Foord EE, Černý P, Jackson LL, Sherman DM, Eby RK (1995) Mineralogical and geochemical evolution of micas from

miarolitic pegmatites of the anorogenic Pikes Peak batholith, Colorado. Miner Petrol 55(1–3):1–26. doi:10.1007/BF01162576

Giuli G, Paris E, Wu ZY, Brigatti MF, Cibin G, Mottana A, Marcelli A (2001) Experimental and theoretical XANES and EXAFS study of tetra-ferriphlogopite. Eur J Miner 13:1099–1108. doi:10.1127/0935-1221/2001/0013-1099

Kile DE, Foord EE (1998) Micas from the Pikes Peak batholith and its cogenetic granitic pegmatites, Colorado: optical properties, composition, and correlation with pegmatite evolution. Can Miner 36(2):463–482

Krause MO, Oliver JH (1979) Natural widths of atomic K and L levels, Kα X-ray lines and several KLL Auger lines. J Phys Chem Ref Data 8(2):329–338. doi:10.1063/1.555595

Longworth G, Townsend MG, Provencher R, Kodama H (1987) Magnetic interaction in biotites and oxidised biotites. Phys Chem Miner 15(1):71–77. doi:10.1007/BF00307611

Marcelli A, Cibin G, Di Matteo S, Chaboy J, Di Gioacchino D, Tripodi P, Brigatti MF, Mottana A (2004) Octahedral low spin symmetric configurations vs. high spin octahedral distorted configurations: the case of Fe in natural layered silicates. J Phys Chem Sol 65:1491–1500. doi:10.1016/j.jpcs.2003.11.04

Meyrowitz R (1970) New semi-microprocedure for determination of ferrous iron in refractory silicate minerals using a sodium metafluoborate decomposition. Anal Chem 42:1110–1113. doi:10.1021/ac60291a021

Nespolo M, Ďurovič S (2002) Crystallographic basis of polytypism and twinning in micas. In: Mottana A, Sassi FP, Thompson JB Jr, Guggenheim S (eds) Micas: crystal chemistry and metamorphic petrology, vol 46. Mineralogical Society of America, Washington, DC, pp 155–272. doi:10.2138/rmg.2002.46.04

Rancourt DG, Christie IAD, Lamarche G, Swainson I, Flandrois S (1994) Magnetism of synthetic and natural annite mica: ground state and nature of excitations in an exchange-wise two-dimensional easy-plane ferromagnet with disorder. J Magn Magn Mater 138:31–44. doi:10.1016/0304-8853(94)90396-4

Rieder M, Cavazzini G, D'yakonov YS, Frank-Kamenetskii VA, Gottardi G, Guggenheim S, Koval PV, Müller G, Neiva AMR, Radoslovich EW, Robert J-L, Sassi FP, Takeda H, Weiss Z, Wones DR (1998) Nomenclature of the micas. Clays Clay Miner 41:61–72

Sheldrick GM (1997) SHELX-97, program for crystal structure determination. University of Göttingen, Germany

Tombolini F, Marcelli A, Mottana A, Cibin G, Brigatti MF, Giuli G (2002) Crystal chemical study by XANES of trioctahedral micas: the most characteristic layer silicates. Int J Mod Phys B Condens Matter Phys Statist Phys Appl Phys 16:1673–1679

Townsend MG (1987) 'Comment on magnetism in biotites' by O. Ballet. Replay. Phys Chem Miner 13(4):282–283. doi:10.1007/BF00308282

Townsend MG, Longworth G (1985) Sign of the magnetic coupling of iron (2+) and iron (3+) ions in biotite. Phys Chem Miner 12:141–144. doi:10.1007/BF00308206

Townsend MG, Longworth G, Ross CAM, Provencher R (1987) Ferromagnetic or antiferromagnetic iron III spin configurations in sheet silicates. Phys Chem Miner 15:64–70. doi:10.1007/BF00307610

Unruh DM, Snee LW, Foord EE, Simmons WB (1995) Age and cooling history of the Pikes Peak batholith and associated pegmatites. Geol Soc Am Abstr Program 27A:468

Waychunas GA, Apted MJ, Brown GE Jr (1983) X-ray K-edge absorption spectra of Fe minerals and model compounds: near edge structure. Phys Chem Miner 10(1):1–9. doi:10.1007/BF01204319

Wilke M, Farges F, Petit PE, Brown GE Jr, Martin F (2001) Oxidation state and coordination of Fe in minerals: an Fe K-XANES spectroscopic study. Am Miner 86(5–6):714–730